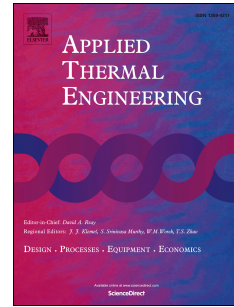


# Accepted Manuscript

Energy and geotechnical behaviour of energy piles for different design solutions

Niccolò Batini, Alessandro F. Rotta Loria, Paolo Conti, Daniele Testi, Walter Grassi, Lyesse Laloui



PII: S1359-4311(15)00394-4

DOI: [10.1016/j.applthermaleng.2015.04.050](https://doi.org/10.1016/j.applthermaleng.2015.04.050)

Reference: ATE 6570

To appear in: *Applied Thermal Engineering*

Received Date: 26 January 2015

Revised Date: 30 March 2015

Accepted Date: 21 April 2015

Please cite this article as: N. Batini, A.F. Rotta Loria, P. Conti, D. Testi, W. Grassi, L. Laloui, Energy and geotechnical behaviour of energy piles for different design solutions, *Applied Thermal Engineering* (2015), doi: 10.1016/j.applthermaleng.2015.04.050.

This is a PDF file of an unedited manuscript that has been accepted for publication. As a service to our customers we are providing this early version of the manuscript. The manuscript will undergo copyediting, typesetting, and review of the resulting proof before it is published in its final form. Please note that during the production process errors may be discovered which could affect the content, and all legal disclaimers that apply to the journal pertain.

# Energy and geotechnical behaviour of energy piles for different design solutions

Niccolò Batini<sup>+</sup>, Alessandro F. Rotta Loria<sup>+</sup>, Paolo Conti<sup>^^</sup>, Daniele Testi<sup>^^</sup>, Walter Grassi<sup>^^</sup>  
and Lyesse Laloui<sup>+</sup>

<sup>+</sup> Swiss Federal Institute of Technology in Lausanne, EPFL, Laboratory of Soil Mechanics  
EPFL-ENAC-IIC-LMS, Station 18, 1015 Lausanne, Switzerland

<sup>^^</sup> University of Pisa, Department of Energy, Systems, Territory and Constructions  
Engineering, DESTEC, Building Energy Technique and TEchnology Research group,  
BETTER, Largo Lucio Lazzarino, 56122 Pisa, Italy

\*Corresponding author: alessandro.rottaloria@epfl.ch

## Abstract

Energy piles are heat capacity systems that have been increasingly exploited to provide both supplies of energy and structural support to civil structures. The energy and geotechnical behaviours of such foundations, which are governed by their response to thermo-mechanical loads, is currently not fully understood, especially considering the different design solutions for ground-coupled heat exchangers. This paper summarises the results of numerical sensitivity analyses that were performed to investigate the thermo-mechanical response of a full-scale energy pile for different (i) pipe configurations, (ii) foundation aspect ratios, (iii) mass flow rates of the fluid circulating in the pipes and (iv) fluid mixture compositions. This study outlines the impacts of the different solutions on the energy and geotechnical behaviour of the energy piles along with important forethoughts that engineers might consider in the design of such foundations. It was observed that the pipe configuration strongly influenced both the energy and the geotechnical performance of the energy piles. The foundation aspect ratio also played an important role in this context. The mass flow rate of the fluid circulating

30 in the pipes remarkably influenced only the energy performance of the foundation. Usual  
31 mixtures of a water-antifreeze liquid circulating in the pipes did not markedly affect both the  
32 energy and the geotechnical performance of the pile.

33

34 **Keywords:** Energy piles; thermo-mechanical behaviour; energy performance; geotechnical  
35 performance; design configurations.

36

## 37 **1. Introduction**

38 Energy piles (EP) are a relatively new technology that couples the structural role of canonical  
39 pile foundations to that of heat exchangers. These foundations, already needed to provide  
40 structural support to the superstructure, are equipped with pipes with a heat carrier fluid  
41 circulating into them to exploit the large thermal storage capabilities of the ground for the  
42 heating and cooling of buildings and infrastructures, particularly when these EPs are coupled  
43 to heat pumps. In these systems, heat is exchanged between the foundations and the soil in a  
44 favourable way, as the undisturbed temperature of the ground at a few meters of depth  
45 remains relatively constant throughout the year (being warmer than the ambient temperature  
46 in the winter and cooler in the summer) and the thermal storage capacities of both media are  
47 advantageous for withstanding the process. Geothermal heat pumps are connected to the piles  
48 and can transfer the stored heat and their energy input to buildings and infrastructures during  
49 the heating season. On the contrary, they can extract the heat from the conditioned spaces and  
50 inject it (again, in addition to their energy input) to the soil during the cooling season.  
51 Temperature values that are adequate to reach comfort levels in living spaces and  
52 advantageous for engineering applications (e.g., de-icing of infrastructures) can be achieved  
53 through this technology with a highly efficient use of primary energy. Traditionally,

54 geothermal borehole heat exchangers have been exploited for this purpose. Recently, the use  
55 of energy piles has been increasingly spreading because of the savings in the installation costs  
56 related to their hybrid character and to the drilling process.

57 The EPs possess a twofold technological character that has drawn a dual related scientific  
58 interest in their behaviour. In fact, the energy performance of the energy piles can markedly  
59 vary for different *(i)* site layouts, *(ii)* foundation geometries, *(iii)* pipe configurations, and *(iv)*  
60 soil and foundation material properties. In addition, the geotechnical behaviour of the energy  
61 piles can strongly vary for different *(v)* restraint conditions and *(vi)* applied thermal loads.  
62 Consequently, these two fundamental aspects of the energy piles are interconnected and  
63 coupled through the thermal and mechanical responses of these foundations.

64 Over the years, a number of studies have investigated the thermal behaviour of vertical  
65 ground-coupled heat exchangers, focusing on the processes that occur inside (i.e., the tubes,  
66 infill material and fluid) and around (i.e., the surrounding soil) their domain. Analytical [1-11]  
67 and numerical [12-31] models of varying complexity have been developed for such purposes.  
68 Currently, various amounts of research have been increasingly performed for the analysis of  
69 the thermal behaviour of energy piles [32-49]. However, the three-dimensional, asymmetric  
70 and time-dependent characterisation of the thermal behaviour of such foundations, which  
71 involves the interaction between the fluid in the pipes, the pipes themselves, the pile and the  
72 surrounding soil, has often been considered in simplified ways that have been deepened only  
73 for specific case studies and have not been coupled with the mechanics of the problem. This  
74 latter aspect, i.e., the variation of the mechanical behaviour of both the foundation and the soil  
75 surrounding the energy piles due to thermal loads, has been investigated in recent years  
76 through several numerical studies in the field of civil engineering [50-60]. However, except  
77 for some of the very latest research [61, 62], these studies generally simplified the numerical  
78 modelling of the complex thermal behaviour of the energy piles by imposing temperature

79 variations or thermal powers to the entire modelled foundations, which were considered to be  
80 homogeneous solids, without the inner pipes and the circulating fluid. From a geotechnical  
81 and structural engineering point of view, this approach put the analyses on the side of safety  
82 (especially in the short-term) because the entire foundation undergoes the highest temperature  
83 variation and hence the maximum induced mechanical effect. However, from an energy  
84 engineering point of view, the physics governing the real problem has been markedly  
85 approximated. In particular, when dealing with models in which ground heat exchangers are  
86 coupled to the other building-plant sub-systems within a global thermodynamic and energetic  
87 analysis [63-65], the aforementioned simplifications may lead to inaccurate performance  
88 predictions and non-optimal design choices.

89 Energy piles, because of their bluntness, should be analysed as capacity systems capable of  
90 responding to a phase shift in a variation of the boundary conditions. More specifically, the  
91 thermal behaviour of the foundation should be investigated considering the complex pipes-  
92 pile-soil system as the heat exchange problem is governed by the temperature differences  
93 between these components. Together with these aspects, the coupled transient mechanical  
94 behaviour of the foundation should be analysed as it governs the bearing response for the  
95 superstructure. In this framework, looking at a thorough assessment of the interplay between  
96 the thermal and mechanical behaviour of energy piles, the present paper summarises the  
97 results of a series of 3-D numerical sensitivity analyses comprising the considered aspects for  
98 a single full-scale energy pile. This study is performed with reference to the features of the  
99 energy foundation of the Swiss Tech Convention Centre at the Swiss Federal Institute of  
100 Technology in Lausanne (EPFL), and investigates the roles of different *(i)* pipe  
101 configurations, *(ii)* foundation aspect ratios, *(iii)* mass flow rates of the working fluid, and *(iv)*  
102 fluid mixture compositions on the transient thermo-mechanical response of energy piles. This  
103 investigation focuses hence on the influence between the thermal and mechanical behaviours

104 of energy piles under transient conditions considering different technical solutions applicable  
105 to such foundations. The adherence to physical reality characterising the numerical approach  
106 considered herein is corroborated by satisfying numerical predictions [66] of experimental  
107 tests [67, 68] that have been recently performed at the site of interest.

108 The foundation is tested during its heating operation mode (the superstructure is heated while  
109 the ground is cooled). With respect to the considered design solutions, the energy  
110 considerations related to (i) the thermal response of the foundation in the short-term, (ii) the  
111 time constants for approaching the steady state conditions of the heat exchange and (iii) the  
112 heat transferred between the fluid in the pipes and the surrounding system are presented.  
113 Geotechnical aspects related to (iv) the stress distribution in the pile and (v) the displacements  
114 fields characterising the foundation depth are also considered.

115 In the following sections, the key features characterising the finite element modelling of the  
116 examined problem are first presented. The results of the numerical sensitivity analyses are  
117 then outlined. Finally, the thermo-mechanical behaviour of the energy piles and the related  
118 energy and geotechnical performances are discussed with reference to the simulated design  
119 solutions.

120

## 121 **2. 3-D finite element modelling of an energy pile**

### 122 **2.1 The simulated site**

123 The dimensions of the energy pile and the characteristics of the surrounding soil deposit  
124 considered in this study are those of an experimental site located at the Swiss Federal Institute  
125 of Technology in Lausanne (EPFL), under the recently built Swiss Tech Convention Centre.  
126 The experimental site includes a group of four energy piles installed below a corner of a

127 heavily reinforced raft supporting a water retention tank. The foundation of the tank includes,  
128 besides the four energy piles, eleven other conventional piles that are not equipped as heat  
129 exchangers [67, 68]. This study considers only one of the four energy piles with respect to a  
130 configuration denoted by a null head restraint and a null mechanical applied load on the top of  
131 the foundation, i.e., the one before the construction of the water tank. The energy pile is  
132 characterised by a height  $H_{EP} = 28$  m and a diameter  $D_{EP} = 0.90$  m (see Figure 1). The pipes  
133 in the shallower 4 meters are thermally insulated to limit the influence of the external climatic  
134 conditions on the heat exchange process. The characteristics of the soil deposit surrounding  
135 the piles (see again Figure 1) are similar to those reported by Laloui et al. [53] as the  
136 considered energy foundation is placed in close proximity to the one referred in this study.  
137 The ground water table at the test site is at the top of the deposit. The upper soil profile  
138 consists of alluvial soil for a depth of 7.7 m. Below this upper layer, a sandy gravelly moraine  
139 layer is present at the depth between 7.7-15.7 m. Then, a stiffer thin layer of bottom moraine  
140 is present at a depth between 15.7-19.2 m. Finally, a molasse layer is present below the  
141 bottom moraine layer.

142

## 143 **2.2 Mathematical formulation and constitutive models**

144 To develop a quantitative description of the response of the energy pile in the considered soil  
145 deposit under the mechanical and thermal loads, the following assumptions were made: (i) the  
146 soil layers were considered to be isotropic, fully saturated by water and assumed to be purely  
147 conductive domains with equivalent thermo-physical properties given by the fluid and the  
148 solid phases, (ii) both the liquid and the solid phases were incompressible under isothermal  
149 conditions, (iii) the displacements and the deformations of the solid skeleton were able to be  
150 exhaustively described through a linear kinematics approach in quasi-static conditions (i.e.,

151 negligible inertial effects), (iv) drained conditions were satisfied during the analysed loading  
 152 processes, and (v) both the soil and energy pile behaved as linear thermo-elastic materials.  
 153 Assumptions (i-iii) have been widely accepted in most practical cases. Hypotheses (iv-v) were  
 154 considered to be representative of the analysed problem in view of the experimental evidence  
 155 that was obtained through *in-situ* tests performed at the site [68, 69]. Therefore, under these  
 156 conditions, a coupled thermo-mechanical mathematical formulation has been employed in the  
 157 following analyses.

158 Assuming Terzaghi's formulation for the effective stress, the equilibrium equation can be  
 159 written as

$$160 \quad \nabla \cdot \sigma'_{ij} + \nabla p_w + \rho g_i = 0 \quad (1)$$

161 where  $\nabla \cdot$  denotes the divergence;  $\nabla$  represents the gradient;  $\sigma'_{ij} = \sigma_{ij} - p_w \delta_{ij}$  denotes the  
 162 effective stress tensor (where  $\sigma_{ij}$  is the total stress tensor,  $p_w$  is the pore water pressure and  
 163  $\delta_{ij}$  is Kroenecker's delta);  $\rho = n\rho_w + (1 - n)\rho_s$  represents the bulk density of the porous  
 164 material, which includes the density of water  $\rho_w$  and the density of the solid particles  $\rho_s$ ,  
 165 through the porosity  $n$ ; and  $g_i$  the gravity vector. The increment of effective stress can be  
 166 expressed as

$$167 \quad d\sigma'_{ij} = C_{ijkl}(d\varepsilon_{kl} + \beta' I_{kl} dT) \quad (2)$$

168 where  $C_{ijkl}$  is the stiffness tensor that contains the material parameters, i.e., the Young's  
 169 modulus,  $E$ , and Poisson's ratio,  $\nu$ ;  $d\varepsilon_{kl}$  is the total strain increment;  $\beta'$  is a vector that  
 170 contains the linear thermal expansion coefficient of the material,  $\alpha$ ;  $I_{kl}$  is the identity matrix;  
 171 and  $dT$  is the temperature increment.

172 As previously mentioned, the ground and the concrete filling of the EP were assumed to be  
 173 purely conductive media. With these assumptions, the energy conservation equation reads



$$174 \quad \rho c \frac{\partial T}{\partial t} - \nabla \cdot (\lambda \nabla T) = 0 \quad (3)$$

175 where  $c$  is the specific heat (including water and solid components  $c_w$  and  $c_s$ );  $t$  is the time;  
 176 and  $\lambda$  is the thermal conductivity (including water and solid components  $\lambda_{p,w}$  and  $\lambda_{p,s}$ ). In  
 177 equation (3), the first term represents the transient component of the internal energy stored in  
 178 the medium and the second term represents the heat transferred by conduction (i.e., through  
 179 Fourier's law). In the considered engineering application, the thermal properties of the fluid  
 180 components were considered to be temperature dependent, whereas those of the solid  
 181 components were considered to be temperature independent.

182 The energy conservation equation for the incompressible fluid flowing in the EP pipes can be  
 183 written as

$$184 \quad \rho_f c_f A_p \frac{\partial T_{bulk,f}}{\partial t} + \rho_f c_f A_p u_{f,i} \cdot \nabla (T_{bulk,f}) = \nabla \cdot [A_p \lambda_f \nabla (T_{bulk,f})] + \dot{q}_p \quad (4)$$

185 where  $\rho_f$ ,  $c_f$ ,  $A_p$ ,  $T_{bulk,f}$ ,  $u_{f,i}$ ,  $\lambda_f$  are the density, specific heat, pipe cross sectional area, bulk  
 186 temperature, longitudinal velocity vector and thermal conductivity of the operative fluid,  
 187 respectively;  $\dot{q}_p$  represents the heat flux per unit length exchanged through the pipe wall and  
 188 is given by

$$189 \quad \dot{q}_p = UP_p(T_{ext} - T_{bulk,f}) \quad (5)$$

190 where  $U$  is an effective value of the pipe heat transfer coefficient,  $P_p = 2\pi r_{int}$  is the wetted  
 191 perimeter of the cross section, and  $T_{ext}$  is the temperature at the outer side of the pipe. The  
 192 overall heat transfer coefficient, including the internal film resistance and the wall resistance,  
 193 can be obtained as follows:

$$194 \quad U = \frac{1}{\frac{1}{h_{int}} + \frac{r_{int}}{\lambda_p} \ln\left(\frac{r_{ext}}{r_{int}}\right)} \quad (6)$$

195 where  $h_{int} = Nu \lambda_f / d_h$  is the convective heat transfer coefficient inside the pipe,  $\lambda_p$  is the  
 196 thermal conductivity of the pipe,  $r_{ext}$  and  $r_{int}$  are the external and internal radii, respectively,  
 197  $d_h = 4A_p/P_p$  is the hydraulic diameter, and  $Nu$  is the Nusselt number. For a given geometry,  
 198  $Nu$  is a function of the Reynolds,  $Re$ , and Prandtl,  $Pr$ , numbers, with

$$199 \quad Nu = \max(3.66; Nu_{turb}) \quad (7)$$

$$200 \quad Nu_{turb} = \frac{(f_D/8)(Re-1000)Pr}{1+12.7\sqrt{f_D/8}(Pr^{1/4}-1)} \quad (7.b)$$

$$201 \quad f_D = \left[ -1.8 \log_{10} \left( \frac{6.9}{Re} \right) \right]^{-1} \quad (7.c)$$

202 where

$$203 \quad Re = \frac{\rho_f u_f d_h}{\mu_f} \quad Pr = \frac{\mu_f c_f}{\lambda_f}$$

204 Equation (7.b) is the Gnielinski formula [70] for turbulent flows; the friction factor,  $f_D$ , is  
 205 evaluated through the Haaland equation [71], which is valid for very low relative roughness  
 206 values.

207

### 208 **2.3 3-D finite element model features**

209 The analyses presented in this study employed the software COMSOL Multiphysics [72],  
 210 which is a finite element simulation environment. In the following sections, sensitivity  
 211 analyses were conducted with respect to three different base-case models of a single energy  
 212 pile equipped with a single U, a double U, and a W-shaped type configuration of the pipes.  
 213 Extra-fine meshes of 107087, 88597 and 98357 elements were used to characterise the models  
 214 for the different foundations. Tetrahedral, prismatic, triangular, quadrilateral, linear and vertex  
 215 elements were employed to describe the  $50D_{EP} \cdot 2H_{EP} \cdot 2H_{EP}$  3-D finite element models.

216 Figure 2 reports the features of a typical model utilised in the study with a focus on the mesh  
217 used to characterise the pile that was equipped with different pipe configurations. The energy  
218 pile was described by 49824, 66722, and 70970 elements for the single U, double U, and W-  
219 shaped type configurations, respectively. The soil surrounding the pile was then characterised  
220 by the remaining 57263, 21875, and 27387 elements for the various models. Tetrahedral  
221 elements were used near the joints of the pipes, whereas the remaining domain of the pile was  
222 covered by means of the swept method. The pipes were simulated with a linear entity in  
223 which the fluid was supposed to flow. In all of the cases, the centres of the pipes were placed  
224 at a distance of 12.6 cm from the boundary of the foundation. Fluid flow inside of the pipes  
225 and the associated convective heat transfer was simulated by an equivalent solid [73], which  
226 possessed the same heat capacity per unit volume (i.e., specific heat multiplied by bulk  
227 density) and thermal conductivity as the actual circulation fluid.

228

#### 229 **2.4 Boundary and initial conditions**

230 Restrictions were applied to both the vertical and horizontal displacements on the base of the  
231 mesh (i.e., pinned boundary) and to the horizontal displacements on the sides (i.e., roller  
232 boundary). The initial stress state due to gravity in the pile and the soil was considered to be  
233 geostatic. The thermal boundary conditions allowed for the heat to flow through the vertical  
234 sides of the mesh and through the bottom of the mesh ( $T_{soil} = 13.2$  °C). The initial  
235 temperatures in the pipes, energy pile and soil were set at  $T_0 = 13.2$  °C, i.e., the average  
236 measured temperature at the considered site during winter. The fluid circulating inside the  
237 pipes (high-density polyethylene tubes) considered in the base-case models was water. The  
238 nominal velocity of the fluid inside the pipes was  $u_f = 0.2$  m/s, and the inner diameter of the  
239 pipes was  $\phi = 32$  mm. In all of the tests, the inflow temperature of the fluid was set at  $T_{in} = 5$

240 °C, which referred to the operation of the energy foundation in winter. A thermal conductivity  
241  $\lambda_p = 0 \text{ W/(mK)}$  was imposed in the shallower 4 meters of the pipes to simulate the thermal  
242 insulation of the ducts near the ground surface. The finite element mesh and the boundary  
243 conditions used in the simulations are shown in Figure 2.

244

## 245 **2.5 Material properties**

246 The soil deposit, energy pile and pipes properties were defined based on the literature review  
247 and in view of the technical documents related to the considered engineering project [53, 67,  
248 69, 74, 75]. They are summarised in Table 1.

249

250

## 251 **3. Thermo-mechanical sensitivity of the energy piles to the different** 252 **technical solutions**

253 The results of different numerical sensitivity analyses considering (i) various pipe  
254 configurations inside of the single energy pile, (ii) foundation aspect ratios, (iii) fluid flow  
255 rates inside the pipes and (iv) fluid compositions are presented in the following sections. The  
256 tests, performed through 3-D transient finite element simulations, occurred over 15 days in  
257 winter. This period has been proven to be sufficient to reach steady-state within the EP  
258 domain: consequently, the enthalpy drop of the fluid from the inlet to the outlet section of the  
259 pipes corresponded to the thermal power exchanged at the EP outer surface (the one in contact  
260 with the soil). Under such conditions, the heat capacity effects were negligible and the energy  
261 pile behaved as a typical heat exchanger that was characterised by an equivalent thermal

262 resistance between the ducts and the soil. The classical effectiveness method for heat  
263 exchangers [76] was used to evaluate and compare the heat transfer process among the  
264 different EP configurations. The heat exchanger effectiveness,  $\varepsilon_{he}$ , is defined as

$$265 \quad \varepsilon_{he} = \frac{T_{out} - T_{in}}{T_{s-p} - T_{in}} \quad (8)$$

266 where  $T_{s-p}$  is the average temperature at the soil-pile interface.

267 Compressive stresses and strains were considered to be positive, as were the downward  
268 displacements (i.e., settlements).

269

### 270 **3.1 Influence of the configuration of the pipes**

271 The thermo-mechanical behaviour of a single energy pile equipped with a single U, a double  
272 U and W-shaped pipes was investigated.

273 Figure 7 shows the axial distributions of the temperature for each type of configuration. As  
274 can be noted, no remarkable temperature variation characterised the shallower 4 meters of the  
275 foundation because the pipes in this region were thermally insulated. After 15 days, the centre  
276 of the foundation equipped with single U, double U and W-shaped pipe configurations  
277 underwent an average cooling of  $\Delta T = T - T_0 = -3.5, -5.5, \text{ and } -5 \text{ }^\circ\text{C}$ , respectively. The  
278 highest temperature variation was reached with the double U-shaped geometry of pipes  
279 because it involved the highest quantity of cold water in the heat exchange process. A more  
280 pronounced cooling of the bottom part of the pile was observed due to the lower thermal  
281 conductivity of the molasse layer, which induced a lower heat exchange with the foundation.  
282 The temperature distribution along the axial foundation depth did not remarkably vary in all

283 of the cases between 7 and 15 days, indicating that the thermal conditions inside the pile were  
284 already close to steady state during the first week of operation.

285 The axial distributions of stress induced by the above-described temperature variations are  
286 shown in Figure 4 (the initial stress distribution due to the foundation body load was  
287 subtracted). Maximum values of the stress  $\sigma_{v,th} = -800, -1400$  and  $-1300$  kPa were observed  
288 along the axial depths of the foundation for the single U, double U, and W-shaped pipe  
289 configurations, respectively. These results were consistent with the previously observed data  
290 because the configurations of the pipes that led to the greatest negative temperature variations  
291 inside the pile were the configurations for which the greatest stresses were observed from the  
292 foundation thermal contractions. The magnitude of the stress induced by the temperature  
293 variation in the energy pile equipped with the single U-shaped pipe configuration was close to  
294 the one characterising the results obtained by Gashti et al. [62] for a single energy pile tested  
295 in winter conditions with the same type of pipe configuration.

296 Figure 5 shows the axial distribution of the vertical displacements for each configuration.  
297 Consistent with the distributions of the temperature and stress, the greatest effect in terms of  
298 the displacement of the cold flow within the tubes was observed for the pile with the double  
299 U-shaped pipe configuration, whereas the smallest effect was observed in the foundation with  
300 the single U-shaped pipe configuration. Maximum pile settlements  $dz_{th} = 0.28, 0.47$  and  $0.46$   
301 mm were observed for the energy pile equipped with the single U, double U, and W-shaped  
302 pipe configurations, respectively. The null point, which represents the plane where zero  
303 thermally induced displacement occurs in the foundation [69], was close to the bottom of the  
304 energy pile for all of the cases. This occurrence was similarly observed by Gashti et al. [62].

305 The temperature trends of the water circulating in the pipes is reported in Figure 6. As can be  
306 observed, the water temperature linearly increased along the flow direction. However, the

307 slight changes of the slope of the curves indicated that the increase was not uniform because  
308 the spatial progressive increase of the water temperature in the pipe reduced the heat transfer  
309 potential with the soil, which thus led to slower temperature increases. The fluid outflow  
310 temperatures,  $T_{out}$ , were higher for the single U pipe configuration with respect to the double  
311 U configuration, and this can be attributed to a thermal interference that occurred in the latter  
312 solution between the two U pipes within the pile. The highest temperature increase was  
313 obtained for the W-shaped pipe configuration, according to the study proposed by Gao et al.  
314 [34].

315 The trends of the thermal power extracted from the ground for the energy pile equipped with  
316 the different considered pipe configurations for the entire duration of the tests is reported in  
317 Figure 6. Complementary data referring to the end of the simulations (15 days) are finally  
318 summarised in Table 2.

319 A decrease of the thermal power extracted from the ground along the foundation depth,  
320  $\dot{Q}/H_{EP}$ , was observed throughout all of the tests (cf. Figure 7) that was consistent with the  
321 temperature decrease that occurred at the soil-pile interface; however, as already noted, the  
322 time evolution of the extracted thermal power almost reached steady-state after one week of  
323 continuous operation. The highest levels of energy extraction were obtained through the  
324 double U and W-shaped pipe solutions, whereas lower amounts of energy were removed from  
325 the ground through the single U-shaped pipe configuration. These results are quantitatively  
326 reported in Table 2, which shows that after 15 days, the energy pile equipped with the double  
327 U-shaped pipes had a 57% higher heat transfer rate than what was obtained through a single  
328 U-shaped pipe configuration; on the other hand, the former design solution was only 2% more  
329 efficient than the one with the W-shaped pipe. In conclusion, the W-shaped pipe configuration  
330 should be considered to be the best trade-off among the design solutions analysed in this  
331 section, owing to (i) a significantly higher energy extraction with respect to the single U-

332 shaped pipe configuration, which justifies its higher installation cost; and (ii) a negligibly  
333 lower energy extraction with respect to the double U-shaped pipe configuration that was  
334 operated at half of the volumetric flow rate,  $\dot{V}$ , that was globally needed for the latter solution  
335 (thus entailing significantly less pumping power). The reason for such similar thermal  
336 behaviour between the two solutions must be determined by the low effectiveness of these  
337 short ground-coupled heat exchangers,  $\varepsilon$ , that was defined in equation (8); more specifically,  
338 a significant departure from the linear trend of the effectiveness versus heat exchanger surface  
339 (which is double for the W-shaped pipe configuration with respect to each of the two U-legs)  
340 towards saturation was not obtained in the tested configurations.

341

### 342 **3.2 Influence of the foundation aspect ratio**

343 The thermo-mechanical behaviour of a single energy pile with aspect ratios  $AR = H_{EP}/D_{EP} =$   
344 10, 20 and 40 ( $D_{EP} = 0.9\text{ m}$ ) was investigated in the present section. The analyses were  
345 performed with respect to the previously considered pipe configurations, and, in each case,  
346 the results were compared to those of the energy pile that was characterised by the nominal  
347 aspect ratio  $AR = 31$ , which was already simulated in section 3.1.

348 Figure 8 shows the axial temperature distributions for each pile aspect ratio and pipe  
349 configuration. The foundation depth was considered in a dimensionless form by dividing it by  
350 the total height of the pile,  $H_{EP}$ . Different temperature distributions along the vertical  
351 coordinate were observed for the various aspect ratios depending upon the thermal properties  
352 of the various soil layers and, above all, on the relative influence of the upper adiabatic 4  
353 meters. As previously observed, the highest temperature variations (and therefore the highest  
354 axial stresses, strains, and displacements variations) were obtained for the energy pile  
355 equipped with the double U-shaped pipes.



356 The axial distributions of the temperature-induced stress in the pile are shown in Figure 9.  
357 Lower and more homogeneous distributions of the vertical axial stress were observed for the  
358 piles with lower aspect ratios  $AR = 9$  and  $18$ , whereas higher and less homogeneous  
359 distributions were obtained for the foundation characterised by the nominal dimensions  
360 ( $AR = 31$ ) and for the one with the highest aspect ratio  $AR = 36$ . This result was due to (i) the  
361 different bearing behaviour that characterised the foundation in the various considered cases,  
362 i.e., predominantly frictional results were observed until an approximate depth of  $20$  m and a  
363 more pronounced end-bearing characteristic was observed from a depth of  $20$  m on and (ii)  
364 due to the impact of the thermal properties of the various soil layers on the heat exchange  
365 process and on the related thermally induced stress. Upper bound values of the axial stress  
366  $\sigma_{v,th} = -926, -1531$  and  $-1513$  kPa were reached in the bottom half of the deeper and more  
367 constrained foundation for the single U, double U, and W-shaped pipe configurations,  
368 respectively. Lower bound values of the axial stress  $\sigma_{v,th} = -181, -300$  and  $-261$  kPa were  
369 reached close to the centre of the shallower and less constrained foundation for the same pipe  
370 configurations.

371 The effect of the different foundation constraints and thermal properties of the various soil  
372 layers can also be observed in Figure 10, which showed the thermal vertical displacements  
373 along the dimensionless foundation depths for the different aspect ratios. The null point  
374 location was close to the geometrical centre of the foundation for the aspect ratios  $AR = 9$  and  
375  $18$ , whereas it was close to the bottom for the aspect ratios  $AR = 31$  and  $36$ . This result  
376 outlines the more pronounced end-bearing behaviour of the foundation for depths greater than  
377  $20$  m, where the molasse layer was found and a higher fraction of the load was transferred to  
378 the pile toe. Upper bound values of the settlements  $dz_{th} = 0.3, 0.7$  and  $0.65$  mm were  
379 observed for the deeper foundation for the single U, double U, and W-shaped pipe  
380 configurations, respectively. Lower bound values of the settlements  $dz_{th} = 0.27, 0.47$  and

381 0.47 mm were observed for the shallower foundation that was equipped with the same pipe  
382 configurations.

383 The distribution of water temperature inside the pipes for the entire duration of the tests and  
384 the useful data related to the energy performance of the piles at the end of the analyses are  
385 finally summarised in Figure 11 and Table 3, respectively. The curvilinear coordinate  
386 following the pipe axis was expressed in dimensionless form by dividing it by the total length  
387 of the pipe,  $x$ . As can be observed in Figure 11, the temperature of the operative fluid in the  
388 pipes increased with the aspect ratio of the pile, obviously due to the increase in the heat  
389 transfer surface. The results of the simulations conducted at the nominal aspect ratio were  
390 consistent with the other results, as observed by the fact that the thermal power that was  
391 extracted from the ground with the double U-shaped pipes was the largest among the analysed  
392 solutions and was followed, in order, by the pile equipped with the W and single U-shaped  
393 pipes (cf. Table 3). A doubling of the foundation aspect ratio from 10 to 20 involved an  
394 increase of the thermal power extraction between 152% and 170% depending on the  
395 configuration of the pipes (the thermally uninsulated surface of the pile was increased by  
396 172%), whereas a doubling from 20 to 40 resulted in a lower relative increase between 87%  
397 and 100% (the uninsulated surface was increased by 127%), which can be attributed to the  
398 tendency of the heat exchanger to become saturated with the increase in the heat transfer  
399 surface.

400

### 401 **3.3 Influence of the fluid flow rate circulating in the pipes**

402 The thermo-mechanical behaviour of a single energy pile characterised by different fluid flow  
403 rates circulating in the pipes was investigated in the present section. Because the fluid flow  
404 rate can change both by a variation of the tube diameter,  $\phi$ , and by the fluid velocity,  $u_f$ , the

405 following numerical analyses considered both options through two different series of tests.  
406 First, the response of the energy pile equipped with pipes of different diameters with water  
407 flowing at a constant velocity was considered. Then, the response of the energy pile equipped  
408 with tubes of the same diameter but that were characterised by different velocities of the  
409 circulating fluid was investigated. The analyses were performed with respect to the previously  
410 considered pipe configurations, and in each case, the results were compared to those of the  
411 energy pile characterised by the nominal features.

412

413

#### 414 **3.3.1 Pipe diameter variations**

415 The axial temperature distributions obtained for the varying pipes diameters ( $\phi = 25$  and  $40$   
416 mm) with respect to the nominal conditions ( $\phi = 32$  mm) and for the different pipe  
417 configurations are shown in Figure 12. A significant decrease of the pile axial temperature  
418 with respect to nominal conditions (approximately  $1$  °C) was observed only for the W-shaped  
419 pipe configuration and for the pipe with the largest diameter (and therefore with the highest  
420 flow rate).

421 The uniform temperature distributions along the foundation depth led to small variations of  
422 the axial stress distributions for the different pipe diameters and configurations. In accordance  
423 with the temperature profile, the more pronounced variations were noted for the energy pile  
424 equipped with the W-shaped pipe where the use of the tubes with diameter  $\phi = 40$  mm  
425 involved an increase of approximately  $-200$  kPa of axial vertical stress with respect to the  
426 nominal conditions (cf. Figure 13).

427 The distribution of the water temperature inside the pipes after 15 days and the trend of  
428 thermal power extracted from the ground for the entire duration of the tests are reported  
429 Figure 14 as a function of the pipe diameters. Complementary data referring to the end of the  
430 simulations are summarised in Table 4.

431 Figure 14 showed an increase in the outflow temperature when the diameter of the pipe was  
432 reduced, and this was attributed to the subsequent decrease in the flow rate. The most  
433 important effect that was observed by the variation of the pipe diameters was with the W-  
434 shaped pipe. The trend of thermal power extracted from the ground showed that besides its  
435 decay with time, up to 10% of the heat transfer rate was gained when the diameter of the pipes  
436 was increased from 25 to 40 mm (cf. Table 4).

437

### 438 **3.3.2 Fluid velocity variations**

439 The axial temperature distributions obtained by varying the water velocities in the pipes  
440 ( $u_f = 0.5$  and  $1$  m/s) with respect to the nominal condition ( $u_f = 0.2$  m/s) and for the  
441 different pipe configurations are shown in Figure . A significant lowering of the pile axial  
442 temperature with respect to the nominal conditions (approximately  $1$  °C) was observed for  
443 only the W-shaped pipe configuration, where the fluid velocity was increased from  $0.2$  to  $0.5$   
444 m/s.

445 In accordance with the uniform temperature distributions along the foundation depth that were  
446 observed for the piles characterised by the single U and double U-shaped pipes, no  
447 remarkable variations of the axial stress distributions were noted in Figure 16. In addition to  
448 the more pronounced variations with respect to the response of the foundation with nominal  
449 features, higher fluid velocities  $u_f = 0.5$  or  $1$  m/s involved an increase of approximately  $-200$   
450 kPa of axial vertical stress for the W-shaped pipe configuration.

451 The distribution of water temperature inside the pipes after 15 days and the trend of thermal  
452 power extracted from the ground for the entire duration of the tests are reported in Figure 17  
453 as a function of the fluid velocities in the pipes. Complementary data referring to the end of  
454 the simulations are summarised in table 5.

455 Figure 17 showed a decrease in the outflow temperature when the water velocity in the pipes  
456 was increased, and this can be attributed to the increase in the flow rate. The trend of thermal  
457 power extracted from the ground showed that despite its typical decay with time, a sensible  
458 growth of the heat transfer efficiency was observed when the fluid velocity increased (cf.  
459 Table 5). In fact, the increase of the water velocity in the pipes from 0.2 to 0.5 m/s created an  
460 increase of approximately 7% in the heat transfer rate and a decrease from 0.2 to 1 m/s  
461 resulted in an increase of approximately 11%. These variations depended upon the  
462 configuration of the pipes, and the most relevant effects were observed for the W-shaped pipe  
463 configuration.

464

### 465 **3.4 Influence of the operating fluid composition**

466 Antifreeze is a chemical additive that lowers the freezing point of a water-based liquid. In  
467 pipes, it is often useful to insert an antifreeze liquid mixed with water to avoid technical  
468 problems especially when dealing with foundation working conditions characterised by very  
469 low temperature regimes.

470 The behaviour of a single energy pile with antifreeze additives of MEG 25 and MEG 50  
471 (mixtures with 25% and 50% of mono-ethylene glycol in water, respectively) in the  
472 circulating fluid in the pipes was investigated in the present section. The analyses were  
473 performed with respect to the previously considered pipe configurations, and, in each case,  
474 the results were compared to those of the energy pile with water circulating in the pipes.

475 The thermal properties of MEG 25 and MEG 50 are reported in Table 6.

476 Figure 18 shows the axial temperature distributions that were obtained along the foundation  
477 depth with the different heat carrier fluids.

478 By varying the working fluid, no appreciable differences in the pile axial temperature  
479 distributions were observed. Therefore, the mechanical response of the foundation was not  
480 expected to markedly vary in terms of the stress or displacements.

481 The distribution of the operative fluid temperature inside the pipes after 15 days and the  
482 trends of thermal power extracted from the ground for the entire duration of the tests are  
483 reported in Figure 19 as a function of the liquid circulating in the pipes. Complementary data  
484 referring to the end of the simulations are summarised in Table 7. The use of the antifreeze  
485 liquids did not appreciably affect the temperature of the fluid in the pipes, but it did induce  
486 variations in the performance of the system energy due to the lower specific heat of the  
487 medium.

488 Table 7 shows that a 25% concentration of MEG in water created a decrease of up to 6% in  
489 the heat transfer rate and that a 50% concentration of MEG created a decrease up to 11% with  
490 respect to the nominal conditions with pure water.

491

#### 492 **4. Concluding remarks**

493 This paper summarises the results of a series of numerical simulations that were performed to  
494 investigate the effects of different design solutions (i.e., different pipe configurations, aspect  
495 ratios of the foundation, fluid flow rates circulating in the pipes, and fluid mixture  
496 compositions) on the energy and geotechnical performance of the energy piles. The study  
497 determined that

- 498
- 499
- 500
- 501
- 502
- 503
- 504
- 505
- 506
- 507
- 508
- 509
- 510
- 511
- 512
- 513
- 514
- 515
- 516
- 517
- 518
- 519
- 520
- 521
- 522
- The configuration of the pipes was the most important factor in the characterisation of the thermo-mechanical behaviour of the energy piles. It was observed that the W-shaped pipe configuration resulted in an increase of up to 54% in the heat transfer rate compared with the single U-shaped configuration at the same flow rate. The double U-shaped pipe configuration, which possessed a double flow rate with respect to the other configurations, resulted in the highest cooling of the concrete with the greatest related stress and displacement distributions. Therefore, it was considered to be a less advantageous solution with respect to the W-shaped pipe configuration both from a thermo-hydraulic and a geotechnical point of view.
  - The increase of the foundation aspect ratio resulted in an approximately linear increase of the exchanged heat that was independent from the configuration of the pipes. However, a lengthening or shortening of the energy pile resulted in markedly diverse responses of the foundation to the thermo-mechanical loads, depending on the impact that the different mechanical and thermal properties of the surrounding soil layers may have had on the bearing response of the pile. In the considered cases, a lower and more homogeneous variation of stresses and displacements along the foundation depth was evidenced for the lower energy pile aspect ratios (i.e.,  $AR = 9$  and  $18$ ), whereas higher and less homogeneous evolutions were observed for the higher aspect ratios (i.e.,  $AR = 31$  and  $36$ ).
  - An increase of up to 11% in the heat transfer rate was obtained by increasing the fluid flow rate (more specifically, increasing the water velocity from 0.2 to 1 m/s) with only slight differences in the results for the different pipe configurations (more evident variations were observed for the W-shaped pipe configuration). No remarkable variations of the vertical stress (and related strain and displacement) distributions in the foundation were observed with the variation in the fluid flow rates.

- 523 • Low concentrations of antifreeze that were mixed with water in the pipes did not  
524 markedly affect the energy performance of the pile with respect to the nominal case  
525 where pure water was used (i.e., the heat transfer rate decreased by approximately 6%  
526 for MEG 25). Only the use of higher concentrations of antifreeze caused considerable  
527 decreases in the heat transfer rates (i.e., a decrease of approximately 11% for MEG  
528 50), but these percentages are hardly needed in practical situations. No remarkable  
529 variations of the vertical stress (and related strain and displacement) distributions in  
530 the foundation were observed with the variation of the heat carrier fluid compositions.
- 531 • In all of the cases, the decay of the thermal power extracted from the ground that was  
532 gained by the operative fluid occurred in the first 5 days of continuous functioning. In  
533 this period, the heat transfer rate decreased up to 30% with respect to the first day of  
534 operation for the energy pile equipped with a single U-shaped pipe and up to 45% for  
535 the foundation characterised by the double U and W-shaped pipe configurations.
- 536 • The choice of the most appropriate design solution for the heat exchange operation of  
537 the energy piles should be considered based on the energy demand of the related  
538 environment with respect to the thermo-hydraulic requirements of the heat pumps and  
539 in consideration of the magnitude of the involved effects from the geotechnical point  
540 of view.

541

## 542 **5. References**

543 [1] Carslaw H, Jaeger J. Conduction of heat in solids. Oxford, United Kingdom: Oxford  
544 University Press, 1986.

545 [2] Ingersoll L, Plass H. Theory of the ground pipe heat source for the heat pump. ASHVE  
546 transactions. 1948;47(7):339-48.



- 547 [3] Claesson J, Eskilson P. Conductive heat extraction to a deep borehole: Thermal analyses  
548 and dimensioning rules. *Energy*. 1988;13(6):509-27.
- 549 [4] Zeng H, Diao N, Fang Z. A finite line - source model for boreholes in geothermal heat  
550 exchangers. *Heat Transfer-Asian Research*. 2002;31(7):558-67.
- 551 [5] Ingersoll LR, Zabel OJ, Ingersoll AC. *Heat conduction with engineering, geological, and*  
552 *other applications*. New York, United States: Mc-Graw Hill, 1954.
- 553 [6] Lamarche L, Beauchamp B. A new contribution to the finite line-source model for  
554 geothermal boreholes. *Energy and Buildings*. 2007;39(2):188-98.
- 555 [7] Bennet J, Claesson J, Hellstrom G. *Multipole method to compute the conductive heat*  
556 *flows to and between pipes in a composite cylinder*. Lund, Sweden: University of Lund, 1987.
- 557 [8] Bandos TV, Montero Á, Fernández E, Santander JLG, Isidro JM, Pérez J, et al. Finite line-  
558 source model for borehole heat exchangers: effect of vertical temperature variations.  
559 *Geothermics*. 2009;38(2):263-70.
- 560 [9] Moch X, Palomares M, Claudon F, Souyri B, Stutz B. Geothermal helical heat  
561 exchangers: Comparison and use of two-dimensional axisymmetric models. *Applied Thermal*  
562 *Engineering*. 2014;73(1):691-8.
- 563 [10] Erol S, François B. Efficiency of various grouting materials for borehole heat  
564 exchangers. *Applied Thermal Engineering*. 2014;70(1):788-99.
- 565 [11] Kupiec K, Larwa B, Gwadera M. Heat transfer in horizontal ground heat exchangers.  
566 *Applied Thermal Engineering*. 2015;75:270-6, doi:10.1016/j.applthermaleng.2014.10.003.

- 567 [12] Eskilson P, Claesson J. Simulation model for thermally interacting heat extraction  
568 boreholes. *Numerical Heat Transfer*. 1988;13(2):149-65.
- 569 [13] Hellström G. *Ground heat storage: thermal analyses of duct storage systems*. Lund,  
570 Sweden: Lund University, 1991.
- 571 [14] Yavuzturk C, Spitler JD. A short time step response factor model for vertical ground loop  
572 heat exchangers. *Ashrae Transactions*. 1999;105(2):475-85.
- 573 [15] Sutton MG, Couvillion RJ, Nutter DW, Davis RK. An algorithm for approximating the  
574 performance of vertical bore heat exchangers installed in a stratified geological regime.  
575 *Ashrae Transactions*. 2002;108(2):177-84.
- 576 [16] Lamarche L, Beauchamp B. New solutions for the short-time analysis of geothermal  
577 vertical boreholes. *International Journal of Heat and Mass Transfer*. 2007;50(7):1408-19.
- 578 [17] Lee C, Lam H. Computer simulation of borehole ground heat exchangers for geothermal  
579 heat pump systems. *Renewable Energy*. 2008;33(6):1286-96.
- 580 [18] Marcotte D, Pasquier P. The effect of borehole inclination on fluid and ground  
581 temperature for GLHE systems. *Geothermics*. 2009;38(4):392-8.
- 582 [19] Marcotte D, Pasquier P. Fast fluid and ground temperature computation for geothermal  
583 ground-loop heat exchanger systems. *Geothermics*. 2008;37(6):651-65.
- 584 [20] Al - Khoury R, Bonnier P, Brinkgreve R. Efficient finite element formulation for  
585 geothermal heating systems. Part I: steady state. *International Journal for Numerical Methods*  
586 *in Engineering*. 2005;63(7):988-1013.

- 587 [21] Al - Khoury R, Bonnier P. Efficient finite element formulation for geothermal heating  
588 systems. Part II: transient. *International Journal for Numerical Methods in Engineering*.  
589 2006;67(5):725-45.
- 590 [22] Signorelli S, Bassetti S, Pahud D, Kohl T. Numerical evaluation of thermal response  
591 tests. *Geothermics*. 2007;36(2):141-66.
- 592 [23] Marcotte D, Pasquier P. On the estimation of thermal resistance in borehole thermal  
593 conductivity test. *Renewable Energy*. 2008;33(11):2407-15.
- 594 [24] Lamarche L, Kaji S, Beauchamp B. A review of methods to evaluate borehole thermal  
595 resistances in geothermal heat-pump systems. *Geothermics*. 2010;39(2):187-200.
- 596 [25] Wang J, Long E, Qin W. Numerical simulation of ground heat exchangers based on  
597 dynamic thermal boundary conditions in solid zone. *Applied Thermal Engineering*.  
598 2013;59(1):106-15.
- 599 [26] Bouhacina B, Saim R, Oztop HF. Numerical investigation of a novel tube design for the  
600 geothermal borehole heat exchanger. *Applied Thermal Engineering*. 2015;79:153-62,  
601 doi:10.1016/j.applthermaleng.2015.01.027.
- 602 [27] Chen Y-P, Sheng Y-J, Dong C, Wu J-F. Numerical simulation on flow field in  
603 circumferential overlap trisection helical baffle heat exchanger. *Applied Thermal*  
604 *Engineering*. 2013;50(1):1035-43.
- 605 [28] Pu L, Qi D, Li K, Tan H, Li Y. Simulation study on the thermal performance of vertical  
606 U-tube heat exchangers for ground source heat pump system. *Applied Thermal Engineering*.  
607 2015;79:202-13. doi:10.1016/j.applthermaleng.2014.12.068.

- 608 [29] Moch X, Palomares M, Claudon F, Souyri B, Stutz B. Geothermal helical heat  
609 exchangers: Coupling with a reversible heat pump in western Europe. *Applied Thermal*  
610 *Engineering*. 2015;81:368-75, doi:10.1016/j.applthermaleng.2015.01.072.
- 611 [30] Zarrella A, Capozza A, De Carli M. Performance analysis of short helical borehole heat  
612 exchangers via integrated modelling of a borefield and a heat pump: A case study. *Applied*  
613 *Thermal Engineering*. 2013;61(2):36-47.
- 614 [31] Balbay A, Esen M. Temperature distributions in pavement and bridge slabs heated by  
615 using vertical ground-source heat pump systems. *Acta Scientiarum Technology*.  
616 2013;35(4):677-85.
- 617 [32] Abdelaziz S, Olgun C, Martin J. Design and operational considerations of geothermal  
618 energy piles. *Geo-Frontiers: Advances in Geotechnical Engineering*. Dallas, Texas, United  
619 States: ASCE, 2011. p. 450-9.
- 620 [33] Kwag BC, Krarti M. Performance of Thermoactive Foundations for Commercial  
621 Buildings. *Journal of Solar Energy Engineering*. 2013;135(4):10.1115/1.4025587.
- 622 [34] Gao J, Zhang X, Liu J, Li KS, Yang J. Thermal performance and ground temperature of  
623 vertical pile-foundation heat exchangers: A case study. *Applied Thermal Engineering*.  
624 2008;28(17):2295-304.
- 625 [35] Krarti M, McCartney JS. Analysis of Thermo-Active Foundations With U-Tube Heat  
626 Exchangers. *Journal of Solar Energy Engineering*. 2012;134(2):10.1115/1.4005755.
- 627 [36] Bozis D, Papakostas K, Kyriakis N. On the evaluation of design parameters effects on  
628 the heat transfer efficiency of energy piles. *Energy and Buildings*. 2011;43(4):1020-9.

- 629 [37] Ozudogru T, Olgun C, Senol A. 3D numerical modeling of vertical geothermal heat  
630 exchangers. *Geothermics*. 2014;51(1):312-24.
- 631 [38] Abdelaziz SL, Ozudogru TY, Olgun CG, Martin II JR. Multilayer finite line source  
632 model for vertical heat exchangers. *Geothermics*. 2014;51(1):406-16.
- 633 [39] Abdelaziz SL, Olgun CG, Martin II JR. Equivalent energy wave for long-term analysis of  
634 ground coupled heat exchangers. *Geothermics*. 2015;53(1):67-84.
- 635 [40] Man Y, Yang H, Diao N, Liu J, Fang Z. A new model and analytical solutions for  
636 borehole and pile ground heat exchangers. *International Journal of Heat and Mass Transfer*.  
637 2010;53(13):2593-601.
- 638 [41] Pahud D, Hubbuch M. Measured thermal performances of the energy pile system of the  
639 dock midfield at Zürich Airport. *European Geothermal Congress*. Unterhaching, Germany:  
640 Bundesverband Geothermie, 2007.
- 641 [42] Pahud D, Matthey B. Comparison of the thermal performance of double U-pipe borehole  
642 heat exchangers measured in situ. *Energy and Buildings*. 2001;33(5):503-7.
- 643 [43] Loveridge F, Amis T, Powrie W. Energy pile performance and preventing ground  
644 freezing. *International Conference on Geomechanics and Engineering*. Seoul, South Korea:  
645 Woodhead Publishing, 2012.
- 646 [44] Brettmann T, Amis T. Thermal Conductivity Analysis of Geothermal Energy Piles.  
647 *Geotechnical Challenges in Urban Regeneration Conference*, Deep Foundations Institute.  
648 London, United Kingdom: ASCE, 2011. p. 499-508.

- 649 [45] Thompson III WH. Numerical Analysis of Thermal Behavior and Fluid Flow in  
650 Geothermal Energy Piles. Blacksburg, United States: Virginia Polytechnic Institute and State  
651 University, 2013.
- 652 [46] Loveridge F, Olgun CG, Brettmann T, Powrie W. The thermal behaviour of three  
653 different auger pressure grouted piles used as heat exchangers. *Geotechnical and Geological*  
654 *Engineering*. 2014;1-17.
- 655 [47] Zarrella A, De Carli M, Galgaro A. Thermal performance of two types of energy  
656 foundation pile: Helical pipe and triple U-tube. *Applied Thermal Engineering*.  
657 2013;61(2):301-10.
- 658 [48] Ozudogru TY, Ghasemi-Fare O, Olgun CG, Basu P. Numerical Modeling of Vertical  
659 Geothermal Heat Exchangers Using Finite Difference and Finite Element Techniques.  
660 *Geotechnical and Geological Engineering*. 2015:1-16.
- 661 [49] Saggi R, Chakraborty T. Thermal analysis of energy piles in sand. *Geomechanics and*  
662 *Geoengineering*. 2014: In print.
- 663 [50] Suryatriyastuti M, Mroueh H, Burlon S. Understanding the temperature-induced  
664 mechanical behaviour of energy pile foundations. *Renewable and Sustainable Energy*  
665 *Reviews*. 2012;16(5):3344-54.
- 666 [51] Knellwolf C, Peron H, Laloui L. Geotechnical analysis of heat exchanger piles. *Journal*  
667 *of Geotechnical and Geoenvironmental Engineering*. 2011;137(10):890-902.
- 668 [52] Mimouni T, Laloui L. Towards a secure basis for the design of geothermal piles. *Acta*  
669 *Geotechnica*. 2014;9(3):355-66.

- 670 [53] Laloui L, Nuth M, Vulliet L. Experimental and numerical investigations of the behaviour  
671 of a heat exchanger pile. *International Journal for Numerical and Analytical Methods in*  
672 *Geomechanics*. 2006;30(8):763-81.
- 673 [54] Olgun CG, Ozudogru TY, Arson C. Thermo-mechanical radial expansion of heat  
674 exchanger piles and possible effects on contact pressures at pile–soil interface. *Géotechnique*  
675 *Letters*. 2014;4(July–September):170-8.
- 676 [55] Ozudogru TY, Olgun CG, Arson CF. Analysis of friction induced thermo-mechanical  
677 stresses on a heat exchanger pile in isothermal soil. *Geotechnical and Geological Engineering*.  
678 2014:1-15.
- 679 [56] Saggi R, Chakraborty T. Cyclic Thermo-Mechanical Analysis of Energy Piles in Sand.  
680 *Geotechnical and Geological Engineering*. 2014:1-22.
- 681 [57] Di Donna A, Laloui L. Numerical analysis of the geotechnical behaviour of energy piles.  
682 *International Journal for Numerical and Analytical Methods in Geomechanics*. 2014, doi:  
683 10.1002/nag.2341.
- 684 [58] Rotta Loria AF, Gunawan A, Shi C, Laloui L, Ng CWW. Numerical modelling of energy  
685 piles in saturated sand subjected to thermo-mechanical loads. *Geomechanics for Energy and*  
686 *the Environment*. 2014, doi: 10.1016/j.gete.2015.03.002.
- 687 [59] Rotta Loria AF, Di Donna A, Laloui L. Numerical study on the suitability of centrifuge  
688 testing the thermal-induced mechanical behavior of energy piles. *Journal of Geotechnical and*  
689 *Geoenvironmental Engineering*. 2014: In print.

- 690 [60] Wang W, Regueiro R, McCartney J. Coupled axisymmetric thermo-poro-mechanical  
691 finite element analysis of energy foundation centrifuge experiments in partially saturated silt.  
692 *Geotechnical and Geological Engineering*. 2014;1-16.
- 693 [61] Olgun CG, Ozudogru TY, Abdelaziz SL, Senol A. Long-term performance of heat  
694 exchanger piles. *Acta Geotechnica*. 2014, doi: 10.1007/s11440-014-0334-z.
- 695 [62] Gashti EHN, Malaska M, Kujala K. Evaluation of thermo-mechanical behaviour of  
696 composite energy piles during heating/cooling operations. *Engineering Structures*.  
697 2014;75(1):363-73.
- 698 [63] Casarosa C, Conti P, Franco A, Grassi W, Testi D. Analysis of thermodynamic losses in  
699 ground source heat pumps and their influence on overall system performance. *Journal of*  
700 *Physics: Conference Series*. 2014;547(012006):1-10.
- 701 [64] Conti P, Grassi W, Testi D. Proposal of a holistic design procedure for ground source  
702 heat pump systems. *European Geothermal Congress*. Pisa, Italy. 2013.
- 703 [65] Conti P, Testi D. Seasonal thermal performance of geothermal piles. *European*  
704 *COMSOL Conference*. Milan, Italy. 2012.
- 705 [66] Di Donna A, Rotta Loria AF, Laloui L. Numerical study on the response of a group of  
706 energy piles under different combinations of thermo-mechanical loads. *Computers and*  
707 *Geotechnics*. 2015: Submitted.
- 708 [67] Mimouni T, Laloui L. Full-scale in situ testing of energy piles. In: Laloui L, Di Donna A,  
709 editors. *Energy geostructures: innovation in underground engineering*: Wiley-ISTE, 2013. p.  
710 23-43.



- 711 [68] Mimouni T, Laloui L. Behaviour of a group of energy piles. Canadian Geotechnical  
712 Journal. 2015: Submitted.
- 713 [69] Laloui L, Moreni M, Vulliet L. Behaviour of a bi-functional pile, foundation and heat  
714 exchanger (in French). Canadian Geotechnical Journal. 2003;40(2):388-402.
- 715 [70] Gnielinski V. New equations for heat and mass transfer in turbulent pipe and channel  
716 flow. International Chemical Engineering. 1976;16(1):359-68.
- 717 [71] Haaland S. Simple and Explicit Formulas for the Friction Factor in Turbulent flow.  
718 Journal of Fluids Engineering – Transactions of the ASME. 1983;103(1):89-90.
- 719 [72] COMSOL. COMSOL Multiphysics version 4.4: user's guide and reference manual.  
720 Burlington, Massachusetts, United States: COMSOL, 2014.
- 721 [73] Lazzari S, Priarone A, Zanchini E. Long-term performance of BHE (borehole heat  
722 exchanger) fields with negligible groundwater movement. Energy. 2010;35(12):4966-74.
- 723 [74] Laloui L, Moreni M, Steinmann G, Fromentin A, Pahud D. Test in real conditions of the  
724 static behaviour of a pile subjected to thermomechanical solicitations (in French). Internal  
725 report. Lausanne, Switzerland: Swiss Federal Institute of Technology in Lausanne (EPFL),  
726 1998.
- 727 [75] Rotta Loria AF, Di Donna A, Laloui L. From in-situ tests to numerical simulations: the  
728 response of an energy pile foundation. Internal report. Lausanne, Switzerland: Swiss Federal  
729 Institute of Technology in Lausanne (EPFL), 2013.
- 730 [76] Lavine A, DeWitt D, Bergman T, Incropera F. Fundamentals of Heat and Mass Transfer.  
731 Hoboken, New Jersey, United States Wiley, 2011.

733

734 **6. List of tables**

735

Soil layer								
	$E$ [MPa]	$\nu$ [-]	$n$ [-]	$\rho$ [kg/m <sup>3</sup> ]	$c$ [J/(kg·K)]	$\lambda$ [W/(m·K)]	$\alpha$ [1/K]	$K$ [m/s]
A1	190	0.22	0.1	2769	880	1.8	$0.33 \times 10^{-5}$	$7 \times 10^{-6}$
A2	190	0.22	0.1	2769	880	1.8	$0.33 \times 10^{-5}$	$1 \times 10^{-5}$
B	84	0.4	0.35	2735	890	1.8	$0.33 \times 10^{-4}$	$1 \times 10^{-5}$
C	90	0.4	0.3	2740	890	1.8	$0.33 \times 10^{-4}$	$2 \times 10^{-10}$
D	3000	0.2	0.1	2167	923	1.11	$0.33 \times 10^{-6}$	$2 \times 10^{-10}$
Energy pile and pipes								
Concrete	28000	0.25	0.1	2500	837	1.628	$1 \times 10^{-5}$	-
HDPE	-	-	-	-	-	0.42	-	-

736 **Table 1: Material properties of the soil deposit, energy pile, and pipes.**

737

738

739

740

741

742

743

744

745

746

747

748

749

750

Pipes configuration	$T_{out}$ [°C]	$\Delta T$ [°C]	$T_{s-p}$ [°C]	$\epsilon_{he}$ [-]	$\dot{V}$ [l/min]	$\dot{Q}/H_{EP}$ [W/m]
Single U-shaped	5.70	0.70	10.73	0.122	9.7	16.9
Double U-shaped	5.55	0.55	9.06	0.135	19.3	26.5
W-shaped	6.08	1.08	9.15	0.260	9.7	26.1

751 **Table 2: Thermal performances of the energy piles for the different pipe configurations.**

752

753

754

755

756

757

758

759

760

761

762

763

764

765

766

767

768

769

770

771

772

<b>Single U-shaped pipe</b>						
$AR$ [-]	$T_{out}$ [°C]	$\Delta T$ [°C]	$T_{s-p}$ [°C]	$\varepsilon_{he}$ [-]	$\dot{V}$ [l/min]	$\dot{Q}/H_{EP}$ [W/m]
10	5.17	0.17	10.85	0.028	9.7	12.5
20	5.44	0.44	10.71	0.077	9.7	16.5
31.1*	5.70	0.70	10.73	0.122	9.7	16.9
40	5.86	0.86	10.65	0.152	9.7	16.1
<b>Double U-shaped pipes</b>						
10	5.14	0.14	9.20	0.032	19.3	20.3
20	5.35	0.35	9.05	0.086	19.3	26.3
31.1*	5.55	0.55	9.06	0.135	19.3	26.5
40	5.69	0.69	8.80	0.182	19.3	25.9
<b>W-shaped pipe</b>						
10	5.28	0.28	9.02	0.070	9.7	21.0
20	5.71	0.71	8.94	0.180	9.7	26.6
31.1*	6.08	1.08	9.15	0.260	9.7	26.1
40	6.33	1.33	8.82	0.347	9.7	24.9

773 \* Base case

774 **Table 6: Thermal performances of the energy piles for the different aspect ratios.**

775

776

777

778

779

780

781

782

783

784

<b>Single U-shaped pipe</b>						
$\phi$ [mm]	$T_{out}$ [°C]	$\Delta T$ [°C]	$T_{s-p}$ [°C]	$\epsilon_{he}$ [-]	$\dot{V}$ [l/min]	$\dot{Q}/H_{EP}$ [W/m]
25	6.07	1.07	10.67	0.189	5.9	15.8
32*	5.70	0.70	10.73	0.122	9.7	16.9
40	5.46	0.46	10.44	0.085	15.1	17.3
<b>Double U-shaped pipes</b>						
25	5.85	0.85	9.03	0.211	11.8	25.0
32*	5.55	0.55	9.06	0.135	19.3	26.5
40	5.36	0.36	8.67	0.098	30.2	27.1
<b>W-shaped pipe</b>						
25	6.64	1.64	9.25	0.386	5.9	24.2
32*	6.08	1.08	9.15	0.260	9.7	26.1
40	5.72	0.72	8.56	0.201	15.1	27.0

785 \* Base case

786 **Table 4: Thermal performances of the energy piles for the different pipe diameters.**

787

788

789

790

791

792

793

794

795

796

797

798

<b>Single U-shaped pipe</b>						
$u_f$ [m/s]	$T_{out}$ [°C]	$\Delta T$ [°C]	$T_{s-p}$ [°C]	$\varepsilon_{he}$ [-]	$\dot{V}$ [l/min]	$\dot{Q}/H_{EP}$ [W/m]
0.2*	5.70	0.70	10.73	0.122	9.7	16.9
0.5	5.29	0.29	10.47	0.052	24.1	17.2
1	5.15	0.15	10.41	0.028	48.3	18.1
<b>Double U-shaped pipes</b>						
0.2*	5.55	0.55	9.06	0.135	19.3	26.5
0.5	5.23	0.23	8.71	0.061	48.3	27.4
1	5.12	0.12	8.67	0.033	96.5	29.0
<b>W-shaped pipe</b>						
0.2*	6.08	1.08	9.15	0.260	9.7	26.1
0.5	5.46	0.46	8.51	0.132	24.1	27.9
1	5.24	0.24	8.38	0.071	48.3	29.0

799 \* Base case

800 **Table 5: Energy performances for the different water velocities circulating inside of the pipes.**

801

802

803

804

805

806

807

808

809

810

811

812

<b>MEG 25</b>				
<b><math>T</math> [°C]</b>	<b><math>\rho_f</math> [kg/m<sup>3</sup>]</b>	<b><math>c_f</math> [J/(kg·K)]</b>	<b><math>\lambda_f</math> [W/(m·K)]</b>	<b><math>\mu_f</math> [Pa·s]</b>
-10	1048	3713	0.477	$3.186 \times 10^{-3}$
-5	1046	3719	0.481	$2.704 \times 10^{-3}$
0	1045	3726	0.485	$2.314 \times 10^{-3}$
5	1044	3734	0.489	$1.995 \times 10^{-3}$
10	1042	3742	0.493	$1.733 \times 10^{-3}$
<b>MEG 50</b>				
-10	1094	3201	0.413	$5.316 \times 10^{-3}$
-5	1092	3221	0.412	$4.428 \times 10^{-3}$
0	1090	3240	0.411	$3.723 \times 10^{-3}$
5	1087	3260	0.410	$3.157 \times 10^{-3}$
10	1084	3280	0.408	$2.700 \times 10^{-3}$

813 **Table 6: Thermal properties of MEG 25 and MEG 50.**

814

815

816

817

818

819

820

821

822

823

824

825

826

<b>Single U-shaped pipe</b>						
<i>Type of antifreeze</i>	$T_{out}$ [°C]	$\Delta T$ [°C]	$T_{s-p}$ [°C]	$\epsilon_{he}$ [-]	$\dot{V}$ [l/min]	$\dot{Q}/H_{EP}$ [W/m]
Pure water*	5.70	0.70	10.73	0.122	9.7	16.9
MEG 25	5.74	0.74	10.59	0.132	10.1	18.6
MEG 50	5.80	0.80	10.65	0.141	10.5	20.9
<b>Double U-shaped pipes</b>						
Pure water*	5.55	0.55	9.06	0.135	19.3	26.5
MEG 25	5.59	0.59	8.96	0.148	20.2	29.6
MEG 50	5.64	0.64	8.94	0.161	21.0	33.4
<b>W-shaped pipe</b>						
Pure water*	6.08	1.08	9.15	0.260	9.7	26.1
MEG 25	6.19	1.19	8.83	0.310	10.1	29.9
MEG 50	6.23	1.23	8.94	0.312	10.5	32.3

827 \* Base case

828 **Table 7: Energy performances for the different operative liquids.**

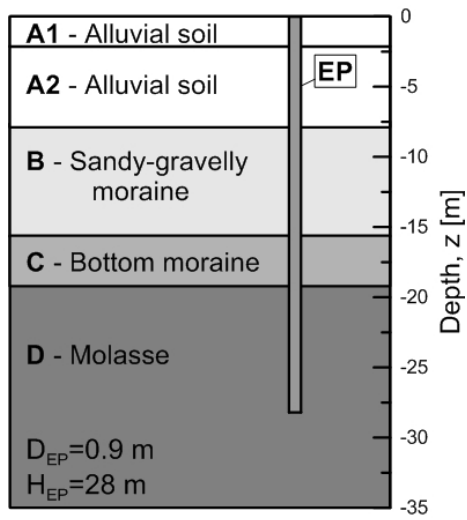
829



830

**7. List of figures**

831



832

833 **Figure 1: Typical soil stratigraphy surrounding the Swiss Tech Convention Centre energy foundation.**

834

835

836

837

838

839

840

841

842

843

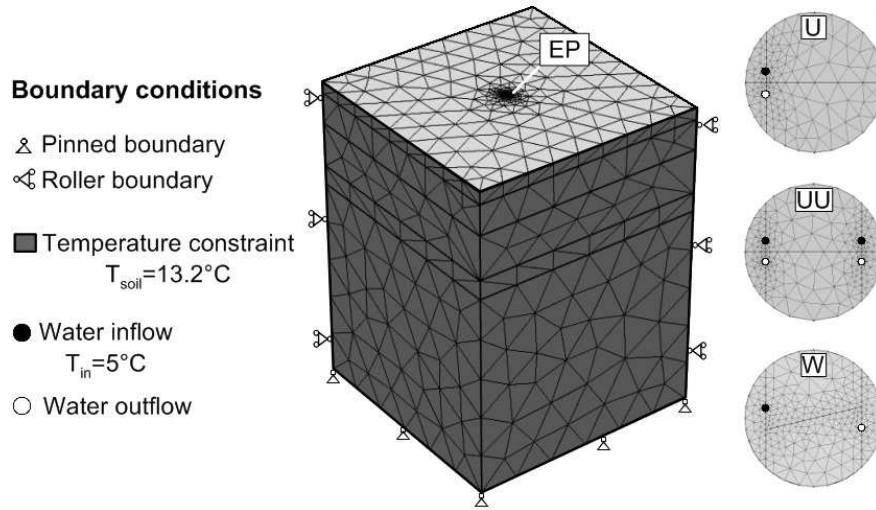
844

845

846

847

848



849

850 **Figure 2: Finite element mesh and boundary conditions used in the simulations.**

851

852

853

854

855

856

857

858

859

860

861

862

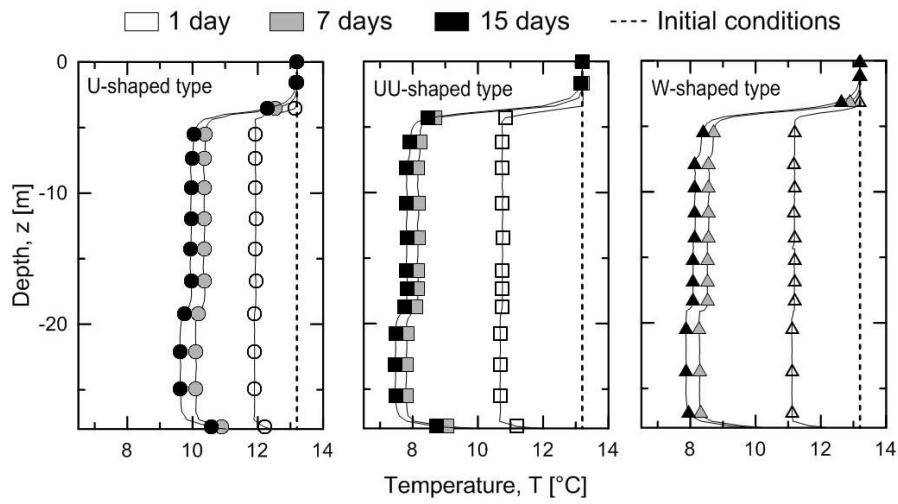
863

864

865

866

867



868

869 **Figure 7: Axial temperature distributions for the different pipe configurations.**

870

871

872

873

874

875

876

877

878

879

880

881

882

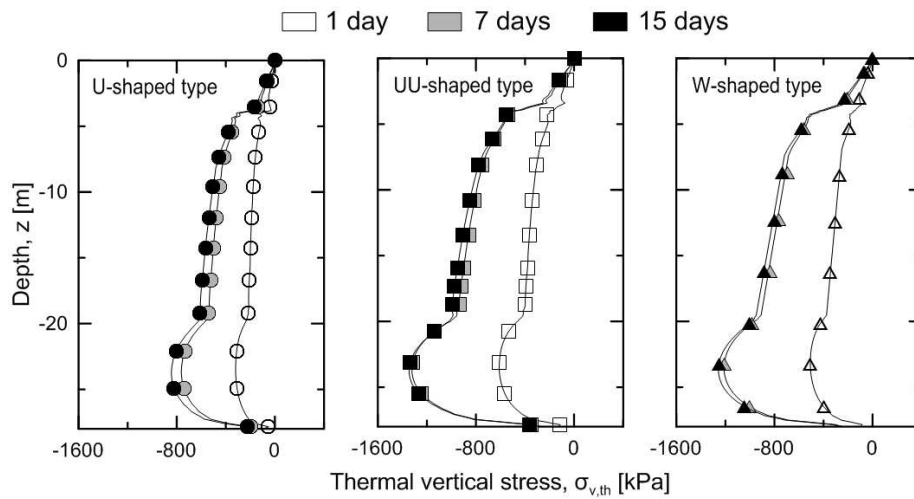
883

884

885

886

887



888

889 **Figure 4: Axial distributions of the thermal vertical stresses for the different pipe configurations.**

890

891

892

893

894

895

896

897

898

899

900

901

902

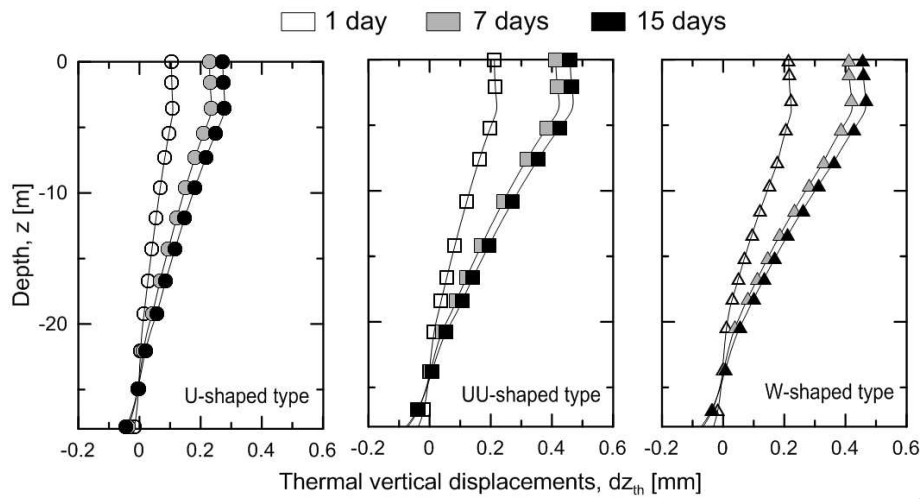
903

904

905

906

907



908

909 **Figure 5: Axial distributions of the thermal vertical displacements for the different pipe configurations.**

910

911

912

913

914

915

916

917

918

919

920

921

922

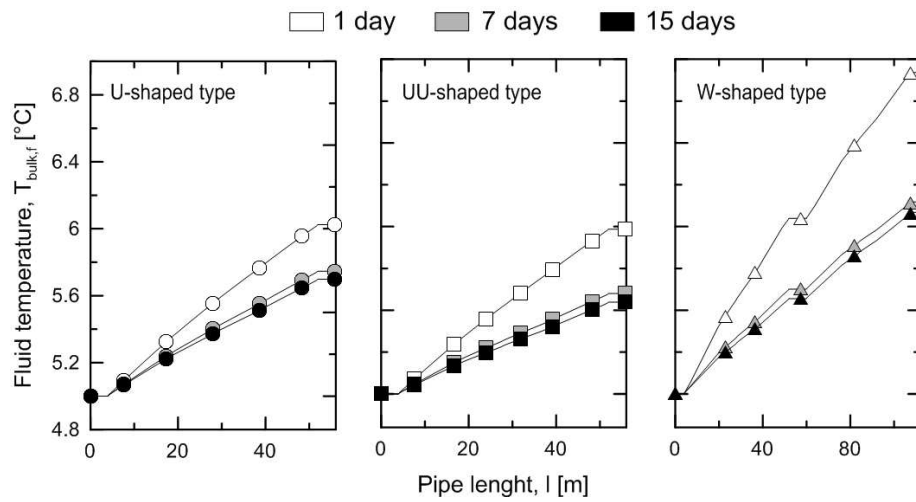
923

924

925

926

927



928

929 **Figure 6: Distributions of the water temperature in the pipes for the different configurations.**

930

931

932

933

934

935

936

937

938

939

940

941

942

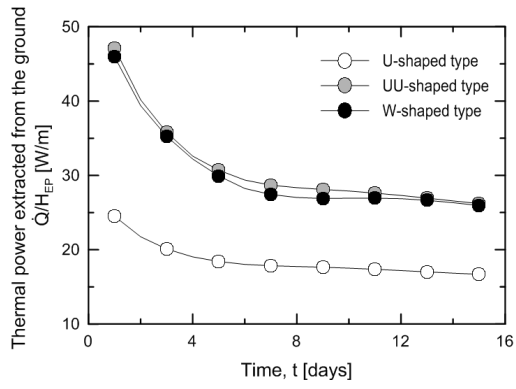
943

944

945

946

947



948

949 **Figure 7: Trend of the thermal power extracted from the ground for the different pipe configurations.**

950

951

952

953

954

955

956

957

958

959

960

961

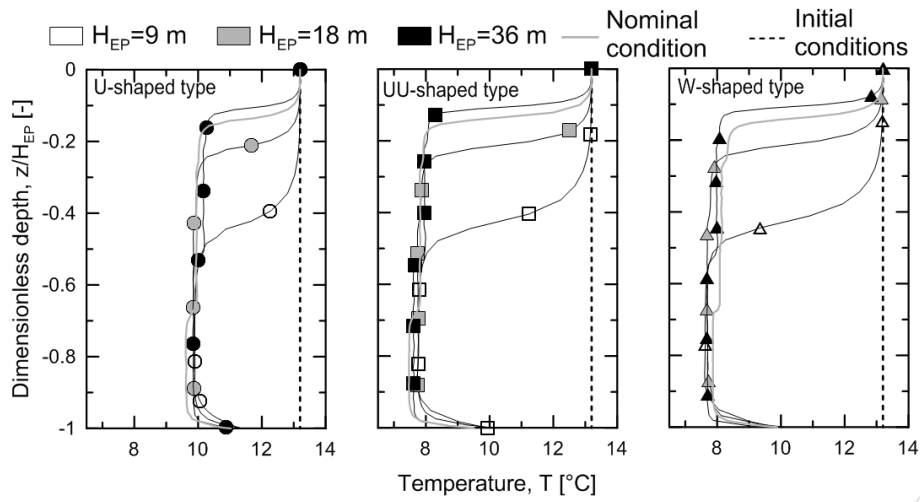
962

963

964

965

966



967

968 **Figure 8: Axial temperature distributions for the different pile aspect ratios.**

969

970

971

972

973

974

975

976

977

978

979

980

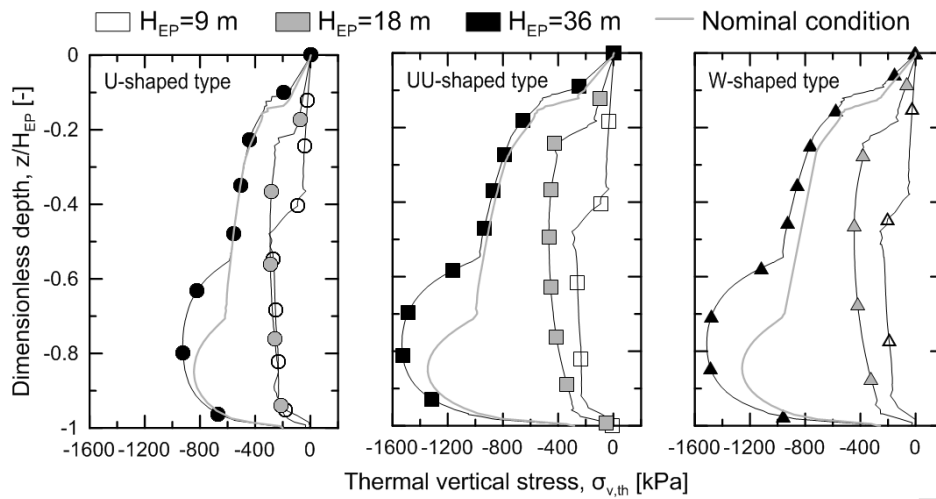
981

982

983

984





985

986 **Figure 9: Axial distributions of the thermal vertical stresses for the different pile aspect ratios.**

987

988

989

990

991

992

993

994

995

996

997

998

999

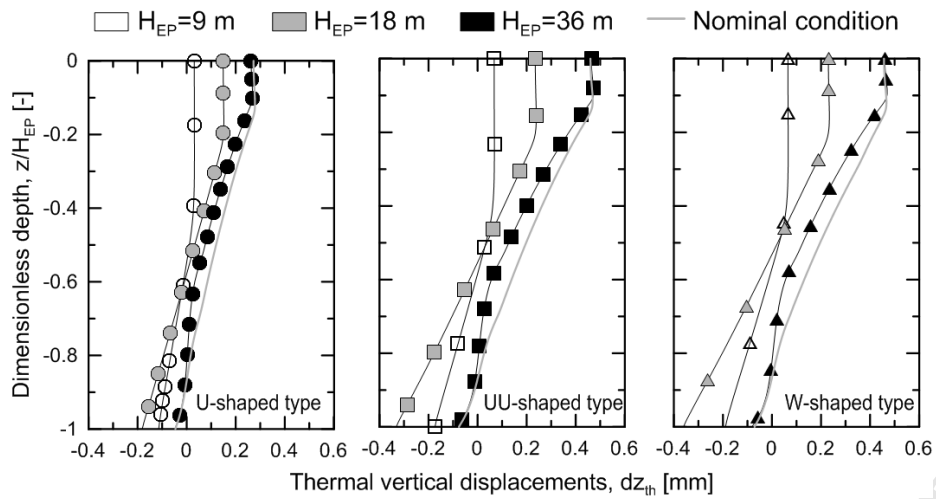
1000

1001

1002

1003

1004



1005

1006

**Figure 10: Axial distributions of the thermal vertical displacements for the different pile aspect ratios.**

1007

1008

1009

1010

1011

1012

1013

1014

1015

1016

1017

1018

1019

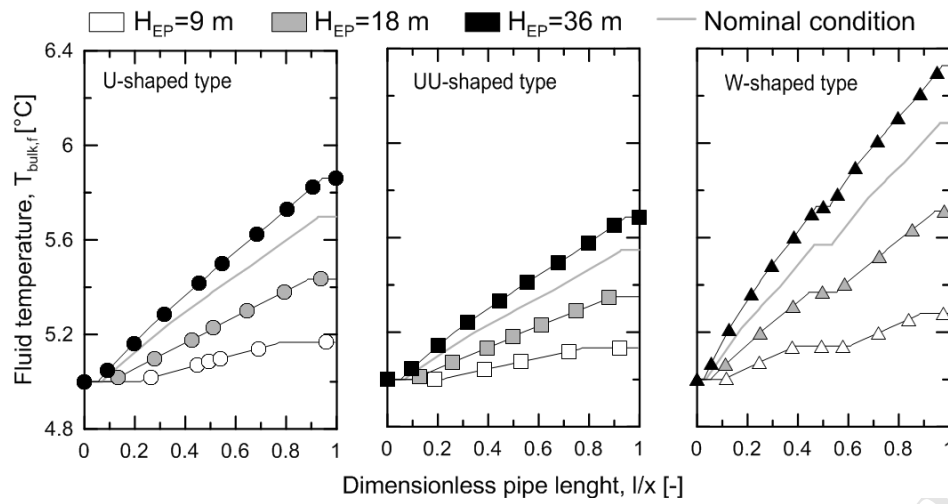
1020

1021

1022

1023

1024



1025

1026 **Figure 11: Distributions of the water temperature in the pipes for the different pile aspect ratios.**

1027

1028

1029

1030

1031

1032

1033

1034

1035

1036

1037

1038

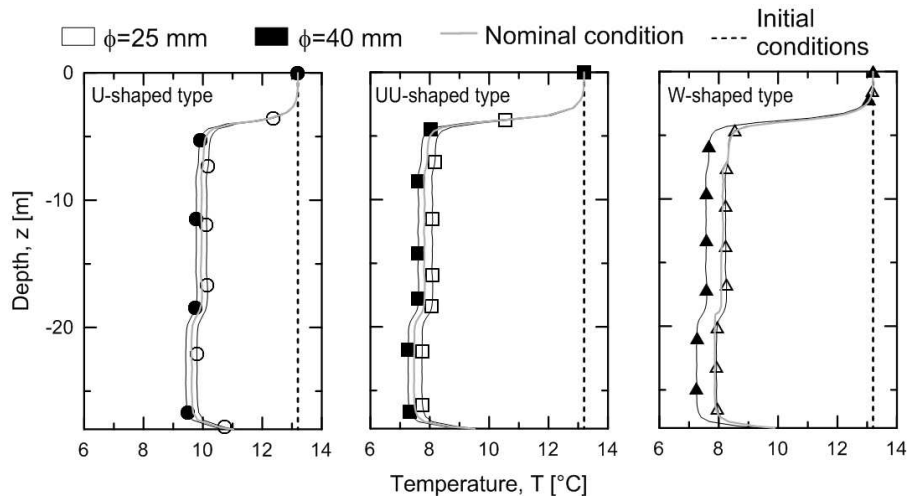
1039

1040

1041

1042

1043



1044

1045 **Figure 12: Axial temperature distributions for the different pipe diameters.**

1046

1047

1048

1049

1050

1051

1052

1053

1054

1055

1056

1057

1058

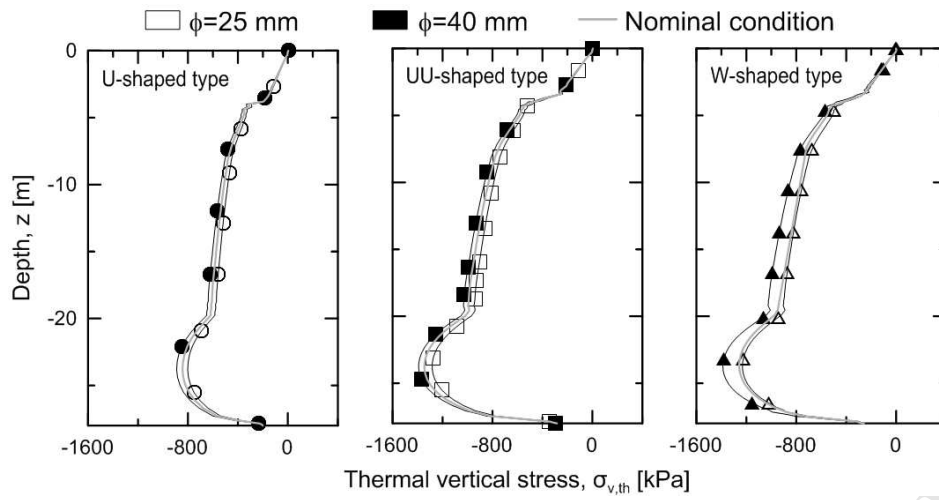
1059

1060

1061

1062

1063



1064

1065 **Figure 13: Axial distributions of the vertical stress for the different pipe diameters.**

1066

1067

1068

1069

1070

1071

1072

1073

1074

1075

1076

1077

1078

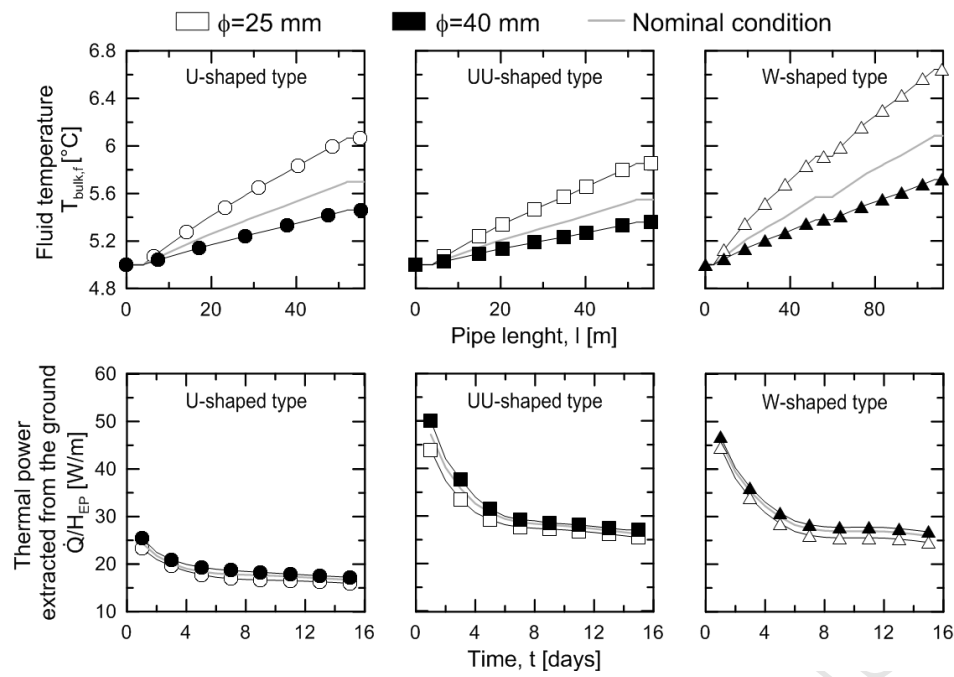
1079

1080

1081

1082

1083



1084

1085 **Figure 34: Distributions of the water temperatures in the pipes for the different pipe diameters and the**  
 1086 **relative trends of the thermal power extracted from the ground.**

1087

1088

1089

1090

1091

1092

1093

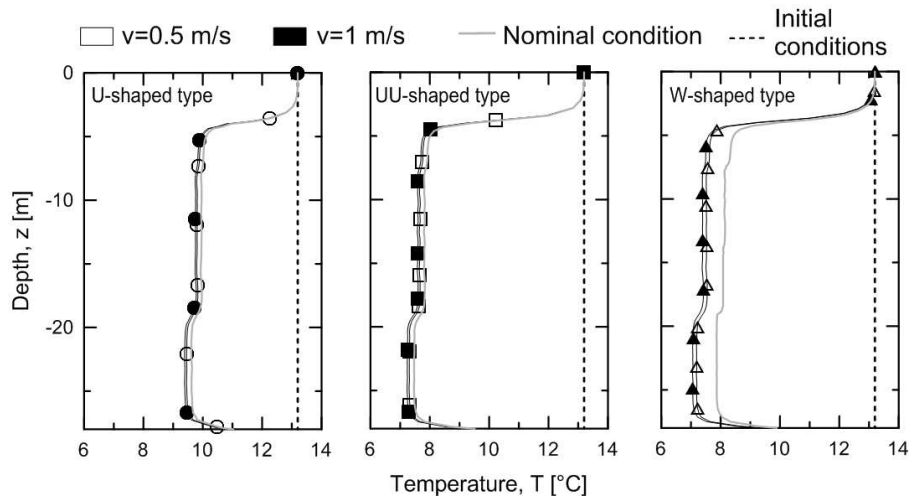
1094

1095

1096

1097

1098



1099

1100 **Figure 15: Axial temperature distributions for the different water velocities.**

1101

1102

1103

1104

1105

1106

1107

1108

1109

1110

1111

1112

1113

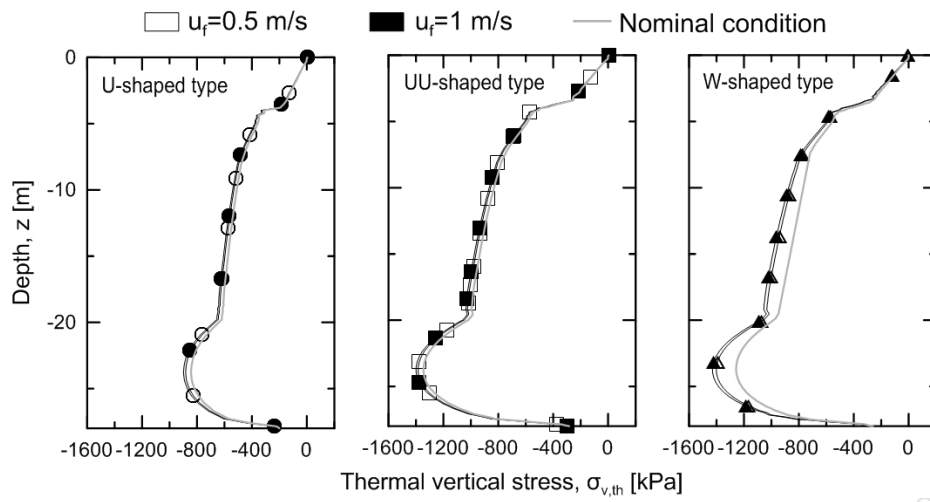
1114

1115

1116

1117

1118



1119

1120 **Figure 16: Axial distributions of the thermal vertical stress for the different water velocities.**

1121

1122

1123

1124

1125

1126

1127

1128

1129

1130

1131

1132

1133

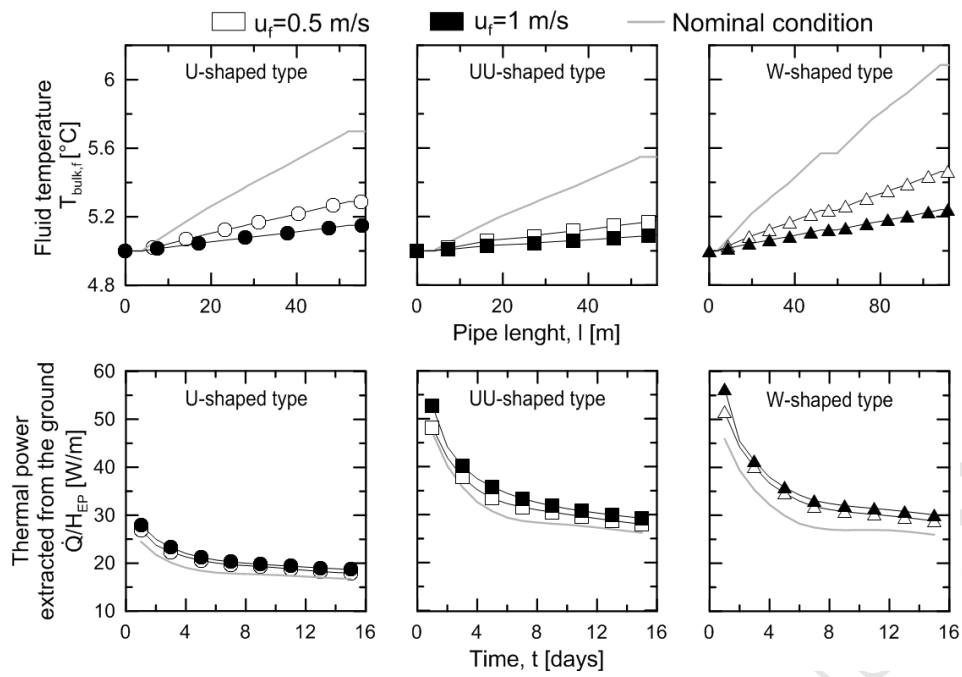
1134

1135

1136

1137





1138

1139 **Figure 17: Distributions of the water temperature in the pipes for the different water velocities and the**  
 1140 **relative trends of the rate of energy extraction from the soil.**

1141

1142

1143

1144

1145

1146

1147

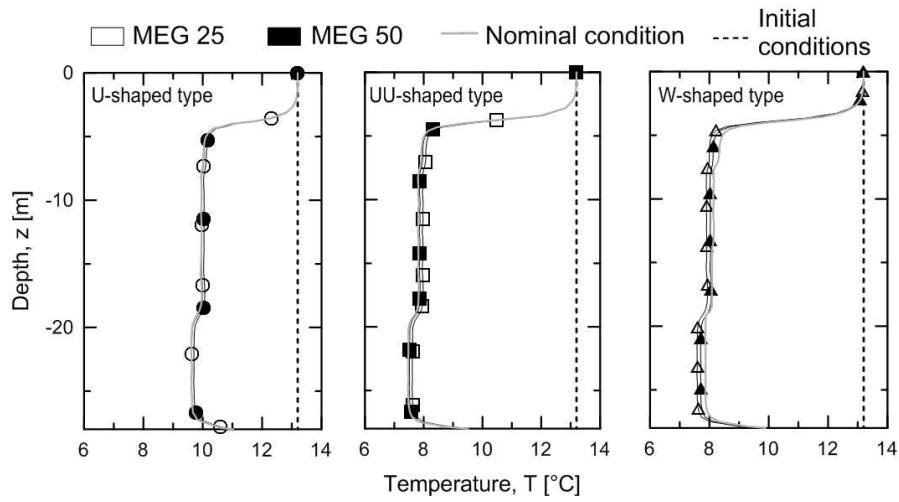
1148

1149

1150

1151

1152



1153

1154 **Figure 18: Axial temperature distributions for the different operative fluids.**

1155

1156

1157

1158

1159

1160

1161

1162

1163

1164

1165

1166

1167

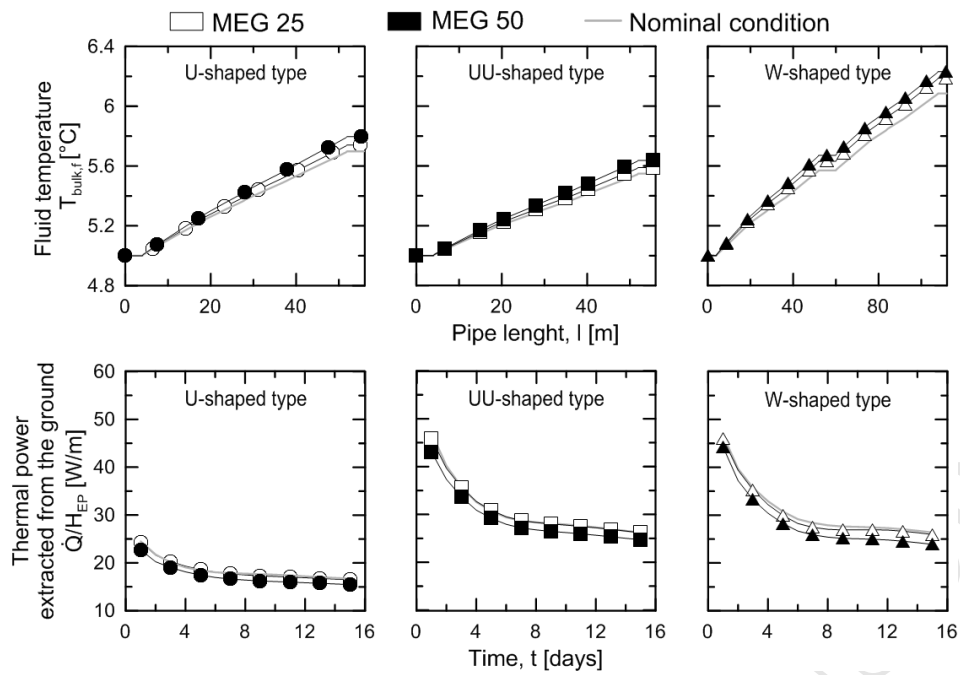
1168

1169

1170

1171

1172



1173

1174 **Figure 19: Distributions of the operative fluid temperatures in the pipes and the relative trends of the**1175 **thermal power extracted from the ground.**



Prof. Lyesse Laloui, Director

Phone/fax: +41(0)216932315/4153

Web: <http://lms.epfl.ch/en>

Applied Thermal  
Engineering  
Editorial Office

Lausanne, 16/03/2015

### Re: Highlights

- Energy piles thermo-mechanical behaviour crucially depends on pipes configuration
- Thermal power extracted from the ground increases with pile aspect ratio
- Heat transfer rate fundamentally depends on fluid mass flow rate
- Heat transfer rate is not markedly affected by operative antifreeze concentrations

Alessandro F. Rotta Loria  
Laboratory for Soil Mechanics